A comparison of water photo-oxidation and photo-reduction using photoelectrodes surface-modified by deposition of co-catalysts: Insights from photo-electrochemical impedance spectroscopy

M. Antuch, W.M.A. El Rouby, P. Millet

A comparison of water photo-oxidation and photo-reduction using photoelectrodes surface-modified by deposition of co-catalysts: insights from photo-electrochemical impedance spectroscopy

M. Antuch[1], W.M.A. El Rouby[1,2], P. Millet[1*]

[1] Paris-Sud University, ICMMO-Eriée, UMR CNRS 8182, 91405 Orsay, France.

[2] Materials Science and Nanotechnology Department, Faculty of Postgraduate Studies for Advanced Science, Beni-Suef University, 62511 Beni-Suef, Egypt.

* Corresponding author e-mail : pierre.millet@u-psud.fr

Abstract

The purpose of this research paper is to highlight mechanistic similarities between water photo-oxidation into molecular oxygen and water photo-reduction into molecular hydrogen, using photoelectrodes surface modified by deposition of co-catalysts. Photo-anodes made of TiO_2 nanorods surface-covered by crystals of cobalt Zeolitic Imidazolate Framework (ZIF-67), and photo-cathodes made of Rh:$SrTiO_3$ particles surface-modified by adsorption of molecules of trisdioximate hexa-chlorine cobalt(II) clathrochelate ($Co(Cl_2Gm)_3(BCH_3)_2$), have been prepared and used for water photo-oxidation and photo-reduction experiments, respectively. Both photoelectrodes have been characterized by SEM and cyclic voltammetry under illumination conditions. Charge transfer mechanisms have been investigated by photo-electrochemical impedance spectroscopy (PEIS). It is shown that for both systems, the presence of a co-catalyst increases the charge transfer kinetics, and that the trapping resistance is larger than the charge transfer resistance, at any operating potential.

Keywords: water photo-oxidation; water photo-reduction; titanium dioxide nanorods; strontium titanate; ZIF-67 MOF.

1. Introduction

The dissociation of water molecules into molecular hydrogen and oxygen is an endergonic chemical reaction of great practical interest for the production or carbon-free energy carriers such as hydrogen [1]. Despite the maturity and efficiency of modern water electrolysers [2] and the possibility to use photovoltaic panels as power source for green hydrogen production [3], the direct photo-dissociation of water into molecular hydrogen and oxygen remains a topic of great practical interest [4-6]. Hydrogen obtained from water in such a way is a solar fuel. It can be produced using either a photochemical reactor (a powder of photoactive material is dispersed in water in a chemical reactor and then illuminated [7]) or a photo-electrochemical reactor (the photoactive powdered material is confined at the surface of a photoelectrode and mounted in a galvanic chain, offering the possibility to apply an external supporting electric bias [8]). In conventional photo-electrochemical cells, the light absorbing semiconducting materials used to design efficient photo-electrodes play a central role. Various strategies such as bulk doping or surface sensitization [9] (*e.g.* by adsorption of organic dyes or other species) have been developed to increase the absorption range of earth-incident sunlight radiations by large band gap materials (*e.g.* titanium dioxide or strontium titanate) for the endergonic water photo-dissociation reaction [10,11]. In the quest for more efficient photon-to-chemical-bonds reaction sequences, charge transfer enhancement via surface co-catalysis is another topic of growing interest. Whereas metallic nano-particles are most commonly used, other materials such as crystals of Metal-Organic Frameworks (MOFs) with tuned redox properties can also be used for that purpose [12]. Ultimately, the implementation of monolayers of electrochemically active molecular complexes deposited at the surface of appropriate semiconducting materials, also offers some interesting perspectives. However, there is a need to go beyond mostly empirical approaches reported so far and to gain knowledge on the interactions between semiconducting substrates and surface co-catalysts in order to improve the charge transfer

kinetics and efficiency. In particular, the role of surface trapping sites [13,14] on the kinetics requires further investigations.

From an experimental viewpoint, photo-electrochemical cells are galvanic chains that are equipped with at least one (sometimes two) photoelectrodes (*i.e.* semiconductor|electrolyte interfaces). From both microscopic and mechanistic viewpoints, the reaction sequences involved in either water photo-oxidation or water photo-reduction are multi-step processes involving the series connection of several microscopic and elementary phenomena such as: light absorption, charge (electron-hole) carriers formation, charge separation and transport to the interfaces, and charge transfer to induce redox transformations. Compared to conventional electrochemical interfaces, kinetics limitations are found within the solid phase (photo-electrode). System improvement requires the detailed analysis of the reaction sequences and the determination of the rate determining step (rds). This can be done for example by measuring photo-electrochemical impedance diagrams on photoelectrodes under illumination, and by modelling experimental data to determine the rate parameter associated to each step. The parasite recombination of charge carriers produced by light absorption at various sites during surface migration should be minimized, while carrier transfer across the interface to the electrolyte should be maximized. In principle, the validity of putative reaction sequences can be tested by using microscopic models. Electrical analogies are very popular for that purpose. Assuming that the photoelectrode/electrolyte interfaces satisfy the necessary conditions of linearity and time invariance, the flux-force relationships are usually described by using electrical resistances and diffusion impedance, and charge accumulation regions are usually described by using electrical capacitances. Microscopic rate parameters can be obtained by fitting experimental impedance data with model equations.

In this context, the purpose of the work reported here was to investigate the role of surface co-catalysis on the kinetics of water photo-oxidation and photo-reduction, to compare the reaction sequences and to discuss the reasons of their kinetics limitations in view of future device

developments. Water photo-oxidation was investigated using titanium dioxide nanorods, surface modified by deposition of a coating of cobalt Zeolitic Imidazole Framework (ZIF) crystals. Water photo-reduction was investigated using rhodium-doped strontium titanate, surface coated by adsorption of cobalt clathrochelate [15]. The behavior of the two systems has been analyzed using the same electrical analogy, an equivalent circuit that may be applied to any type of semiconducting photoelectrode. The role of trapping sites has been put into evidence and analyzed. Despite the obvious differences between these two light-driven water splitting systems (material, type of co-catalyst, bias polarity, light input, half-cell photo-induced reaction), the analysis of the dynamics of charge transfer across these interfaces can thus be systematized in order to gain a coherent perspective of the processes occurring at the semiconductor/electrolyte interface and to facilitate comparisons.

2. Experimental section and model description

2.1. Photoanode: titanium dioxide nanorods modified by deposition of ZIF-67

The water photoanode was prepared as follows. First, titanium dioxide nanorods (TDNRs) were grown on a glass substrate covered by a thin FTO layer, using a well-known and simple hydrothermal method [16] with was slightly modified. Briefly, the FTO-glass substrate was cleaned for approximately 30 mins by ultra-sonication in a mixture of isopropanol, acetone and water (volume ratio 1:1:1), then dried in air and placed in the 50 mL Teflon tubing of a stainless-steel autoclave. Besides this, 15 mL of HCl (37%) were slowly added to 15 mL of milli-Q® grade water in a glassware under continuous stirring, followed by dropwise addition of 0.5 mL of Titanium (IV) butoxide under vigorous stirring. The solution thus obtained was then stirred for 10 mins and poured into the Teflon vessel containing the cleaned FTO-glass substrate. Finally, the hydrothermal growth process itself was performed at 150 °C for 4h. After cooling, the FTO-glass substrate covered by a homogeneous layer of TDNRs was washed by immersion in distilled water 3 times

and then dried in air at room temperature. Then, a coating of ZIF-67 was deposited atop the TDNRs mat using a two-step process: first cobalt electro-reduction and second chemical cobalt transformation into ZIF-67 [17]. Cobalt electrodeposition was performed in a conventional three-electrode cell, using the TDNRs-FTO-glass substrate as working electrode, Saturated Calomel Electrode (SCE) and glassy carbon plate (instead of platinum to avoid contamination) as reference and counter electrodes respectively, and using 25 mL of 0.15 M $CoCl_2 \cdot 6H_2O$ in distilled water as electrolyte. Cobalt electro-deposition was performed by chrono-coulometry at the constant potential of −1.0 V vs SCE for 80 s. The Co- TDNRs array thus obtained was rinsed three times with distilled water. Finally, the cobalt deposit was converted to Co ZIF-67 by immersing the Co-TDNRs array for 4 h in 30 mL of a 1M 2-Methylimidazole solution under continuous stirring. Then, the obtained Co-ZIF-67/TDNRs/FTO-glass photoelectrode was removed from the solution and immersed in distilled water to remove the excess of 2-Methylimidazole and stored in distilled water before utilization.

2.2. Photocathode: rhodium-doped strontium titanate modified by adsorption of cobalt clathrochelate

The technique used for the preparation of $Rh:SrTiO_3$ photoelectrodes has been described elsewhere [15]. Briefly, $Rh:SrTiO_3$ photoelectrodes were prepared by drop-casting 10 μL of an isopropanol suspension containing $Rh:SrTiO_3$ (30 mg in 0.5 mL), on top of a glass substrate covered by a thin FTO layer. 0.5 mL of a 10^{-2} M mother solution of $Co(Cl_2Gm)_2(B\text{-}CH_3)_2$ (M = 575.81 g/mol) was prepared in DMF. 10 μL of this solution was then drop-casted onto the $Rh:SrTiO_3$-covered photoelectrode, corresponding to 10^{-2} μmol (5.8 μg) of cobalt clathrochelate. DMF was then evaporated under a vacuum for two hours, using a primary pump. Next, 10 μL of a Nafion® solution (obtained by diluting 50 μL of the commercial solution in 1 mL of isopropanol) were dropped over the surface using the same methodology, and let dry for one hour. In all cases, the alcoholic solvent was

slowly evaporated at room temperature. Before starting photo-electrochemical measurements, photoelectrodes were put into the electrolyte solution and allowed to wet and equilibrate overnight.

2.3. Photo-electrochemical measurements

All photo-electrochemical measurements have been made in a three-electrode photo-electrochemical cell (Pine Research Instrument Company, USA) equipped with a quartz window, a platinum counter electrode, an SCE, and the working photoelectrodes. A 0.1 M Na_2SO_4 (pH~7) solution was used as liquid electrolyte. Before measurements, the solutions were pupiled by Argon gas for about 30 mins. The light source used was a solar simulator (MAX-303, Asahi Spectra Co.) equipped with a 300 W Xenon lamp for photoanodic processes, and a LED driver (cold white; item MCWHL5) for photocathodic reactions. A Solartron ModuLab XM (USA) potentiostat was used to investigate the photo-electrochemical properties of the photoelectrodes. The photocurrent-potential curves have been measured by varying applied potential from the open circuit potential down/up to -1.3/+1.2 V *vs.* SCE electrode under dark and illumination conditions. Photo-electrochemical impedance spectroscopy (PEIS) spectra were recorded under potentiostatic control and constant illumination. The amplitude of the sinusoidal potential perturbation was set to 10 mV in all cases. Measurements have been made at different potentials *vs.* SCE.

2.4. Electrical analogy

PEIS data measured on the two systems has been analyzed with the support of the electrical analogy of Figure 1-c. This model has a general meaning and may be applied to any type of semiconducting photoelectrode, either photo-cathodes (Figure 1-a) or photo-anodes (Figure 1-b). This model considers that charge transfer to the electrolyte occurs from surfaces states (also called traps) only [18-28]. The direct charge transfer from the conduction or valence bands does not significantly contribute to the current: this is not always the case experimentally but far for being

unusual in such systems. In this model, the charge transfer kinetics is controlled by two resistances. The first resistance (R_{trap}) has two different meanings in the literature: this is the resistance associated to non-Faradaic trapping/detrapping of charge carriers at surface sites [23], but this is sometimes viewed as a resistance related to the parasite electron-hole recombination process promoted by surface states, especially when direct charge transfer from the conduction or valence bands is the main process [22]. Figure 1-c shows that both resistances must be minimized in order to minimize the impedance of the photoelectrode. Therefore R_{trap} has been considered as a trapping resistance of minority carriers in the discussion section and not as a resistance related to recombination. The second resistance (R^{CT}_{trap}), is the charge transfer resistance between surface states and the electrolyte. As shown in Figure 1-c, the charge transfer kinetics is proportional to the concentration of charge carriers on surface states. In addition to that, two capacitances are used to account for carrier storage, either in bulk regions (C_{bulk}) or on trapping sites (C_{trap}). Therefore, the model assumes the existence of two different time constants and it will be shown that this is what is observed experimentally. Best PEIS fits have been obtained using a complex least-square adjustment procedure and corresponding microscopic rate parameters have been deduced from these best fits.

3. Results and discussion

3.1. Water photo-oxidation

Water photo-oxidation experiments were performed using the TDNRs/Co-ZIF-67 photoelectrodes. In this system, conduction band electrons are majority carriers and valence band holes are the minority carriers involved in redox processes at the interface. Figure 2-a shows Scanning Electron Microscopy micrographs of the system. The FTO surface is homogeneously covered with micrometer long TiO_2 nanorods of homogeneous size (inset of Figure 2-a). Figure 2-a also shows the situation after electro-deposition of ZIF-67 MOF atop the TDNRs layer: ZIF-67 crystals are found to be

covering the entire TDNRs mat. A photoelectrode such as the one shown on Figure 2-a, prepared with a 80 s long electro-deposition of cobalt, has been used to photo-oxidize water in a pH-neutral 0.1M Na_2SO_4 solution, as a function of the applied potential. Results obtained under simulated solar light source are shown in Figure 2-b. The experiments, performed under visible light illumination, clearly show the photo-activity of the material and the positive impact that the ZIF-67 deposit has on the overall performances.

Insights into the water photo-oxidation mechanism on this system were gained by photoelectrochemical impedance spectroscopy (PEIS) analysis, performed under constant light irradiation. Experimental PEIS diagrams measured at various electrode potentials are plotted in Nyquist and Bode (imaginary part only) coordinates, in Figure 3-a and 3-b respectively. Impedances reported for TDNRs-ZIF-67 have been measured at lower potentials (400 mV less) than those measured on bare TDNRs, in order to highlight the role of both operating bias and surface co-catalysis. Nyquist plots show somewhat flattened semicircles, indicating that each semicircle has two time constants of close values. Experimental PEIS diagrams were therefore fitted using the electrical analogy of Figure 1-c. The values of the kinetic parameters deduced from the best fits are plotted in Figure 3-c and 3-d, as a function of the applied potential bias. Data show that R_{trap} is larger than R^{CT}_{trap}, for any of the potentials of investigation, with and without ZIF-67 (Figure 3-c). Both resistances tend to decrease logarithmically when the potential bias is increased, indicating an overall hole-to-electrolyte transfer kinetics of increasing rate. Data also show that both resistances (hole trapping and hole transfer) are affected by the presence of the MOF at the interface. The presence of ZIF-67 has a positive effect because the kinetics of hole transfer is increased (reduction of R^{CT}_{trap}). The trapping resistance R_{trap} follows a similar trend, suggesting that charge trapping at the interface was favored too. The trapping capacitance C_{trap} in the presence of ZIF-67 was found to increase while increasing the band bending (Figure 3-d), as observed on other photocatalytic systems [29]. Such behavior, which is predicted by existing models [22], is attributed to the accumulation of holes at the

interface. A shift in peak frequency towards higher frequencies is observed on the Bode plots when the anodic overvoltage is increased. Such trend is related to the potential dependence of the two resistance-capacitance pairs of each time constant, and in particular to the marked potential dependence of the two resistances.

3.2. Water photo-reduction

Water photo-reduction was performed using the Rh:$SrTiO_3$/Co-clathrochelate (Co-Clt for short) photoelectrode. PEIS data reported in this section have been analyzed using the same electrical analogy of Figure 1-c. In this system, valence band holes are majority carriers and photoexcited conduction band electrons are the minority carriers involved in redox processes at the interface. Figure 4-a shows a SEM image of the Rh:$SrTiO_3$ material, covered by a thin film of perfluorosulfonic acid polymer (Nafion®), and containing the cobalt clathrochelate. The Nafion® film cannot be seen on the SEM Figure, because it forms a very thin layer on top of powder particles. Its presence however was confirmed by XPS analysis, during which the cobalt, nitrogen and fluorine contents were clearly put into evidence (not shown here). SEM images taken after photo-electrochemical testing were very similar to those taken before, indicating that photo-electrochemical experiments and potential scans did not cause significant morphological alterations of the photoelectrode surface, at least over the limited duration of the tests. Figure 4-b shows the cyclic voltammograms (CVs) measured under continuous potential cycling at the scan rate of 1 $mV.s^{-1}$ (the standard potential of the HER at this pH is shown as a vertical dotted line). The increasing current measured upon voltage cycling during the first scans suggest either the restructuration of the interface or the possible chemical modification and alteration of the Co-clathrochelate complex at the surface, as reported before for other clathrochelates [30,31]. After approximately a hundred cycles, the CVs become reproducible and stable. Then, the charge transfer process was investigated by photo-electrochemical impedance spectroscopy. The main experimental difference between the two systems

is that the bias is here of opposite sign. Experimental PEIS diagrams measured at various electrode potentials are plotted in Nyquist and Bode (imaginary part only) coordinates in Figure 5-a and 5-b respectively. Nyquist plots (Figure 5-a) again show flattened semicircles and two relaxation constants. This time, the two time constants have different values because two semicircles are sometimes observed. Experimental PEIS diagrams were also fitted using the electrical analogy of Figure 1. Again, microscopic rate parameters were determined from the best fits. As for water photo-oxidation with TiO_2-ZIF-67, the two resistances show a logarithmic variation with applied bias (Figure 5-c) and the charge transfer resistance decreases while increasing the applied potential, indicating an acceleration of the charge transfer process to the electrolyte. The beneficial catalytic effect of the cobalt clathrochelate adsorbed at the surface of Rh:$SrTiO_3$ is not very large but is clearly put into evidence by these data. While R_{trap} is slightly affected by the presence of this surface co-catalyst, the charge transfer resistance decreases, indicating that electron transfer to evolve H_2 is actually being accelerated by the presence of the complex at the interface. The trapping capacitance was found to increase with increasing bias, until a plateau value was obtained (Figure 5-d). As discussed for water photo-oxidation with TDNRs/ZIF-67, this is a usual behavior [22] attributed to the accumulation of electrons at the interface. On the Bode plots, there is almost no frequency shift of the two time constants when the cathodic overvoltage is increased. This is attributed to the counter potential dependence of resistances and capacitances.

3.3. Comparison of both systems

Despite the fact that the two photoelectrodes considered here were significantly different and used for two different photo-electrochemical reactions (water photo-oxidation and water photo-reduction respectively), they both showed similarities in terms of mechanism and kinetic behavior. Both systems can be modeled using the same electrical analogy of Figure 1 which takes into account the existence of surface sites. This is not a new fact but results show that charge trapping sites are present

and disturb charge transfer processes. In both cases the resistances associated to charge trapping and charge transfer exhibited a logarithmic dependence on applied bias. Such relationship is often encountered experimentally and the ratio of the two resistances can be related to the energy depth of the traps [32]. In both systems, the resistance associated to charge trapping was found to be larger than the resistance associated to charge transfer to the electrolyte, indicating that charge trapping is the slowest step in both cases, as explicitly reported earlier for another system [33]. In the case of the TDNRs/ZIF-67 system, the surface co-catalyst (ZIF-67) had a significant and positive impact on R^{CT}_{trap}, but a less pronounced impact on R_{trap}. In the case of the Rh:$SrTiO_3$-Co-Clt system, a different trend was observed: the adsorption of the cobalt clathrochelate at the interface essentially decreased R^{CT}_{trap} but left R_{trap} almost unaffected. The analysis of such effects and the role that surface co-catalysts can play on the trapping resistance is a promising research topic. Further progress will first require the identification of such sites and their location in the surface and sub-surface regions. This will also require specific approaches (for example spectroscopic ones) to quantify trapping energy and investigate the role that surface co-catalysis can play to modulate the value of such energy levels. Regarding the trapping capacitance, results obtained for both systems are similar to those usually encountered experimentally: the increase of surface states capacitances is likely to be related to the surface accumulation of charge carriers [22]. The increasing trapping capacitance is also correlated to the decreasing R^{CT}_{trap} and R_{trap}. This is attributed to the fact that charge accumulation increases the rate of both charge transfer and recombination.

Finally, it should be noted that depending on the type of co-catalyst used in the experiments, the values of both R_{trap} and R^{CT}_{trap} (and hence the impact on the reaction kinetics) will be different [34]. Our objective here was to compare mechanistic aspects of the OER and HER half cell reactions under illumination, to highlight similarities between both processes and to unveil some features on the dynamics of charge transfer versus trapping. A quantitative comparison of our results with best performing co-catalysts is beyond the scope of this paper but the interested reader can look at the

related literature to see what are the main differences in terms of kinetics. An efficient OER co-catalyst reported in the literature is the Ni-Fe Layered Double Hydroxide (LDH) operating in mild or strongly alkaline media [9,35]. The ZIF-67 MOF used here exhibits a lower activity but its impact on the two time constants of the system are clearly shown. Regarding the HER, Pt is the most efficient co-catalyst but its activity is such that the dark current tends to mask the photoactivity of the semi-conducting substrate and make the charge transfer versus trapping analysis more difficult [36]. The Co-clathrochelate used here does not significantly increase the rate and efficiency of the HER on Rh:SrTiO3 but interactions with trapping sites have been evidenced. The activity reported here for this specific system falls within the range of normal photoelectrocatalytic activities, and is even better than some other systems [37].

4. Conclusions

Main conclusions of this work are:

- Photo-anodes made of TiO_2 nanorods surface-covered by crystals of a cobalt Zeolitic Imidazolate Framework (ZIF-67) and photo-cathodes made of Rh:$SrTiO_3$ particles surface-modified by adsorption of trisdioximate hexa-chlorine cobalt clathrochelate ($Co(Cl_2Gm)_3(BCH_3)_2$) have been prepared and used for water photo-oxidation and photo-reduction experiments, respectively.
- For both systems, the surface deposition of co-catalysts was found to increase the kinetics of the respective reaction under consideration.
- In both systems, the trapping resistance was found to be larger than the charge transfer resistance at any operating potential: this is an indication that the flow of minority carriers to the trapping sites is small and that the main kinetic limitation comes from surface trapping in both cases.

- While the presence of ZIF-67 was found to reduce the trapping resistance, that resistance was found to be almost unaffected by the adsorption of cobalt clathrochelate at the surface of strontium titanate. These findings indicate that surface co-catalysts can play a different role in charge transfer kinetics.
- A better characterization of surface trapping sites and a better understanding of the interactions between surface co-catalysts and such surface states will be required in the future, in order to increase the charge transfer kinetics on these systems and to improve their water splitting efficiency.

Acknowledgements

Manuel Antuch is thankful for a French Ministerial Scholarship, and the Initiative d'Excellence (IDEX) Program. Waleed M. A. El Rouby is thankful for the French and Egyptian governments for supporting this work through a co-financed post-doc fellowship granted by the French Embassy in Egypt (Institut Français d'Egypte) and the science and technology development fund (STDF) ID no 30573. Financial support from the French Agence Nationale de la Recherche (research grant CE06-0002-03) is also gratefully acknowledged.

Figure captions

Figure 1. (a) simplified band diagram for a p-type semiconductor/electrolyte interface; (b) likewise for a n-type semiconductor; (c) equivalent circuit model used to simulate experimental PEIS spectra.

Figure 2. (a) SEM micrographs of TDNRs (inset) with ZIF-67 crystals atop; (b) I-V curves measured using TDNRs with (red) and without (black) ZIF-67 crystals, in 0.1 M Na_2SO_4 (10 mV/s), light power 100 mW/cm^2.

Figure 3. TDNRs and TDNRs/ZIF-67 photoelectrode: (a) PEIS spectra in Nyquist coordinates measured at different working potentials; (b) plots of -Z" of the PEIS spectra *vs.* frequency at different working potentials; (c) Plots of R_{trap} and R^{CT}_{trap} *vs.* working potential; (d) Plot of C_{trap} *vs.* working potential. Light intensity = 101 mW/cm^2.

Figure 4. (a) SEM micrographs of Rh:$SrTiO_3$ particles surface-covered with Co-Clt trapped in a thin Nafion film; (b) I-V curves at 1 $mV.s^{-1}$ on Rh:$SrTiO_3$/Co-Clt in 0.1 M Na_2SO_4 under illumination at 529.03 mW/cm^2.

Figure 5. (a) PEIS spectra of the Rh:$SrTiO_3$ - Clt system in Nyquist coordinates at different potentials; (b) plot of -Z" (PEIS spectra) vs. frequency for the Rh:$SrTiO_3$ - Clt system at different potentials; (c) Plots of R_{trap} and R^{CT}_{trap} vs. working potential measured on Rh:$SrTiO_3$-Clt; (d) Plot of C_{trap} vs. working potential measured on Rh:$SrTiO_3$-Clt.

References

[1] A. Scipioni, A. Manzardo, J. Ren, *Hydrogen Economy: Supply Chain, Life Cycle Analysis and Energy Transition for Sustainability*, Academic Press, 2017.

[2] D. Bessarabov, P. Millet, *PEM Water Electrolysis*, B.G. Pollet Ed., Academic Press, Elsevier, 2018.

[3] K. Fujii, S. Nakamura, M. Sugiyama, K. Watanabe, B. Bagheri, Y. Nakano, *Characteristics of hydrogen generation from water splitting by polymer electrolyte electrochemical cell directly connected with concentrated photovoltaic cell*, Inter. J. Hydrogen Energy, 38 (2013) 14424-14432. doi: 10.1016/j.ijhydene.2013.07.010.

[4] T. Hisatomi, J. Kubota, K. Domen, *Recent advances in semiconductors for photocatalytic and photoelectrochemical water splitting*, Chem. Soc. Rev. 43 (2014) 7520–7535. doi:10.1039/C3CS60378D.

[5] M.H. Elbakkay, W.M.A. El Rouby, S.I. El-Dek, A.A. Farghali, *S-TiO_2/S-reduced graphene oxide for enhanced photoelectrochemical water splitting,* Appl. Surf. Sci. 439 (2018) 1088–1102. doi:10.1016/j.apsusc.2018.01.070.

[6] W.M.A. El Rouby, A.A. Farghali, *Titania morphologies modified gold nanoparticles for highly catalytic photoelectrochemical water splitting*, J. Photochem. Photobiol. A Chem. 364 (2018) 740–749. doi:10.1016/j.jphotochem.2018.07.011.

[7] D.M. Fabian, S. Hu, N. Singh, F.A. Houle, T. Hisatomi, K. Domen, F.E. Osterloh, S. Ardo, *Particle Suspension Reactors and Materials for Solar-Driven Water Splitting*, Energy Environ. Sci. 8 (2015) 2825–2850. doi:10.1039/C5EE01434D.

[8] M. Schreier, J. Luo, P. Gao, T. Moehl, M.T. Mayer, M. Grätzel, *Coordinative immobilization of a molecular catalyst on Cu_2O photocathodes for CO_2 reduction*, J. Am. Chem. Soc. 138 (2016) 1938–1946. doi:10.1021/jacs.5b12157.

[9] R.A. Sayed, S.E. Abd El Hafiz, N. Gamal, Y. GadelHak, W.M.A. El Rouby, *Co-Fe layered double hydroxide decorated titanate nanowires for overall photoelectrochemical water splitting*, J. Alloys Compd. 728 (2017) 1171–1179. doi:10.1016/j.jallcom.2017.09.083.

[10] M. Pavlenko, K. Siuzdak, E. Coy, M. Jancelewicz, S. Jurga, I. Iatsunskyi, *Silicon/TiO_2 core-shell nanopillar photoanodes for enhanced photoelectrochemical water oxidation,* Int. J. Hydrogen Energy, 42(51) (2017) 30076-30085.

[11] S. Saraf, M. Giraldo, H.P. Paudel, T.S. Sakthivel, C Shepard, A. Gupta, M.N. Leuenberger, S. Seal, *Photoelectrochemical analysis of band gap modulated TiO_2 for photocatalytic water splitting,* Int. J. Hydrogen Energy, 42(15) (2017) 9938-9944.

[12] Z. Wang, Z. Jin, G. Wang, B. Ma, ***Efficient hydrogen production over MOFs (ZIF-67) and g-C_3N_4 boosted with MoS_2 nanoparticles***, Int. J. Hydrogen Energy, 43(29) (2018) 13039-13050.

[13] T.-F. Hou, R. Boppella, A. Shanmugasundaram, D. Ha Kim, D.-W. Lee, *Hierarchically self-assembled ZnO architectures: establishing light trapping networks for effective photoelectrochemical water splitting*, Int. J. Hydrogen Energy, 42(22) (2017) 15126-15139.

[14] A. Mumtaz, N. Muti Mohamed, M. Imran Irshad, A. Yar, M. Shuaib Mohamed Saheed, *Mutual effects of extrinsic defects and electronic carbon traps of M-TiO2 (M = V, Co, Ni), nanorod arrays on photoexcited charge extraction of CdS for superior photoelectrochemical activity of hydrogen production*, Int. J. Hydrogen Energy, 43(31) (2018) 14388-14405.

[15] M. Antuch, P. Millet, A. Iwase, A. Kudo, S.A. Grigoriev, Y.Z. Voloshin, *Characterization of Rh:SrTiO$_3$ photoelectrodes surface-modified with a cobalt clathrochelate and their application to the hydrogen evolution reaction*, Electrochim. Acta. 258 (2017) 255–265. doi:10.1016/j.electacta.2017.10.018.

[16] B. Liu, E.S. Aydil, *Growth of oriented single-crystalline rutile TiO$_2$ nanorods on transparent conducting substrates for dye-sensitized solar cells*, J. Am. Chem. Soc. 131 (2009) 3985–3990. doi:10.1021/ja8078972.

[17] T. Zhang, J. Du, H. Zhang, C. Xu, *In-situ Growth of Ultrathin ZIF-67 Nanosheets on Conductive Ti@TiO$_2$/CdS Substrate for High-efficient Electrochemical Catalysis*, Electrochim. Acta. 219 (2016) 623–629. doi:10.1016/j.electacta.2016.10.002.

[18] P. Dias, L. Andrade, A. Mendes, *Hematite-based photoelectrode for solar water splitting with very high photovoltage*, Nano Energy. 38 (2017) 218–231. doi:10.1016/j.nanoen.2017.05.051.

[19] S. Jamali, A. Moshaii, *Improving photo-stability and charge transport properties of Cu$_2$O/CuO for photo-electrochemical water splitting using alternate layers of WO$_3$ or CuWO$_4$ produced by the same route*, Appl. Surf. Sci. 419 (2017) 269–276. doi:10.1016/j.apsusc.2017.04.228.

[20] A. Liu, Y. Zhang, W. Ma, W. Song, C. Chen, J. Zhao, *Facial boron incorporation in hematite photoanode for enhanced photoelectrochemical water oxidation*, J. Photochem. Photobiol. A Chem. 355 (2017) 290–297. doi:10.1016/j.jphotochem.2017.08.045.

[21] F.E. Bedoya-Lora, A. Hankin, I. Holmes-Gentle, A. Regoutz, M. Nania, D.J. Payne, J.T. Cabral, G.H. Kelsall, *Effects of low temperature annealing on the photo-electrochemical performance of tin-doped hematite photo-anodes*, Electrochim. Acta. 251 (2017) 1–11. doi:10.1016/j.electacta.2017.08.090.

[22] S.C. Riha, B.M. Klahr, E.C. Tyo, S. Seifert, S. Vajda, M.J. Pellin, T.W. Hamann, A.B.F. Martinson, *Atomic layer deposition of a submonolayer catalyst for the enhanced photoelectrochemical performance of water oxidation with hematite*, ACS Nano. 7 (2013) 2396–2405. doi:10.1021/nn305639z.

[23] K.J. Pyper, J.E. Yourey, B.M. Bartlett, *Reactivity of $CuWO_4$ in photoelectrochemical water oxidation is dictated by a midgap electronic state*, J. Phys. Chem. C. 117 (2013) 24726–24732. doi:10.1021/jp408434v.

[24] C. Miao, T. Shi, G. Xu, S. Ji, C. Ye, *Photocurrent enhancement for Ti-doped Fe_2O_3 thin film photoanodes by an in situ solid-state reaction method*, ACS Appl. Mater. Interfaces. 5 (2013) 1310–1316. doi:10.1021/am302575p.

[25] S.Y. Lim, D. Han, Y.R. Kim, T.D. Chung, *Photoelectrochemical and Impedance Spectroscopic Analysis of Amorphous Si for Light-Guided Electrodeposition and Hydrogen Evolution Reaction*, ACS Appl. Mater. Interfaces. 9 (2017) 23698–23706. doi:10.1021/acsami.7b04961.

[26] H. Hajibabaei, A.R. Schon, T.W. Hamann, *Interface Control of Photoelectrochemical Water Oxidation Performance with $Ni_{1-x}Fe_xO_y$ Modified Hematite Photoanodes*, Chem. Mater. 29 (2017) acs.chemmater.7b01149. doi:10.1021/acs.chemmater.7b01149.

[27] O. Zandi, A.R. Schon, H. Hajibabaei, T.W. Hamann, *Enhanced Charge Separation and Collection in High-Performance Electrodeposited Hematite Films*, Chem. Mater. 28 (2016) 765–771. doi:10.1021/acs.chemmater.5b03707.

[28] S. Hernández, G. Gerardi, K. Bejtka, A. Fina, N. Russo, *Environmental Evaluation of the charge transfer kinetics of spin-coated $BiVO_4$ thin films for sun-driven water photoelectrolysis*, Appl. Catal. B Environ. 190 (2016) 66–74. doi:10.1016/j.apcatb.2016.02.059.

[29] M. Antuch, P. Millet, A. Iwase, A. Kudo, *The role of surface states during photocurrent switching: Intensity modulated photocurrent spectroscopy analysis of $BiVO_4$ photoelectrodes*, Appl. Catal. B Environ. 237 (2018) 401–408. doi:10.1016/j.apcatb.2018.05.011.

[30] B. Lassalle-Kaiser, A. Zitolo, E. Fonda, M. Robert, E. Anxolabéhère-Mallart, *In Situ Observation of the Formation and Structure of Hydrogen-Evolving Amorphous Cobalt Electrocatalysts*, ACS Energy Lett. 2 (2017) 2545–2551. doi:10.1021/acsenergylett.7b00789.

[31] S. El Ghachtouli, M. Fournier, S. Cherdo, R. Guillot, M.-F. Charlot, E. Anxolabéhère-Mallart, M. Robert, A. Aukauloo, *Monometallic Cobalt − Trisglyoximato Complexes as Precatalysts for Catalytic H_2 Evolution in Water*, J. Phys. Chem. C. 117 (2013) 17073–17077.

[32] L. Bertoluzzi, J. Bisquert, *Equivalent Circuit of Electrons and Holes in Thin Semiconductor Films for Photoelectrochemical Water Splitting Applications*, J. Phys. Chem. Lett. 3 (2012) 2517–2522. doi:10.1021/jz3010909.

[33] W.H. Leng, Z. Zhang, J.Q. Zhang, C.N. Cao, *Investigation of the Kinetics of a TiO_2 Photoelectrocatalytic Reaction Involving Charge Transfer and Recombination through Surface States by Electrochemical Impedance Spectroscopy*, J. Phys. Chem. B. 109 (2005) 15008–15023. doi:10.1021/jp051821z.

[34] J. Joy, J. Mathew, S.C. George, *Nanomaterials for Photoelectrochemical Water splitting. A review*, Int. J. Hydrogen Energy, 43(10) (2018) 4804-4817.

[35] M. Gong, Y. Li, H. Wang, Y. Liang, J.Z. Wu, J. Zhou, J. Wang, T. Regier, F. Wei, H. Dai, *An Advanced Ni−Fe Layered Double Hydroxide Electrocatalyst for Water Oxidation*, J. Am. Chem. Soc., 135(23) (2013) 8452-8455.

[36] M. Antuch, P. Millet, A. Iwase, A. Kudo, *Water reduction into hydrogen using Rh-doped $SrTiO_3$ photoelectrodes surface-modified by minute amounts of Pt: Insights from heterogeneous kinetic analysis*, Electrochim. Acta, in press.

[37] L. Gong, L. Wang, J. Lu, C. Han, W. Chen, C. Haur Saw, *Photocurrent Response in Multiwalled Carbon Nanotube Core–Molybdenum Disulfide Shell Heterostructures*, J. Phys. Chem. C 119(43) (2015) 24588−24596.

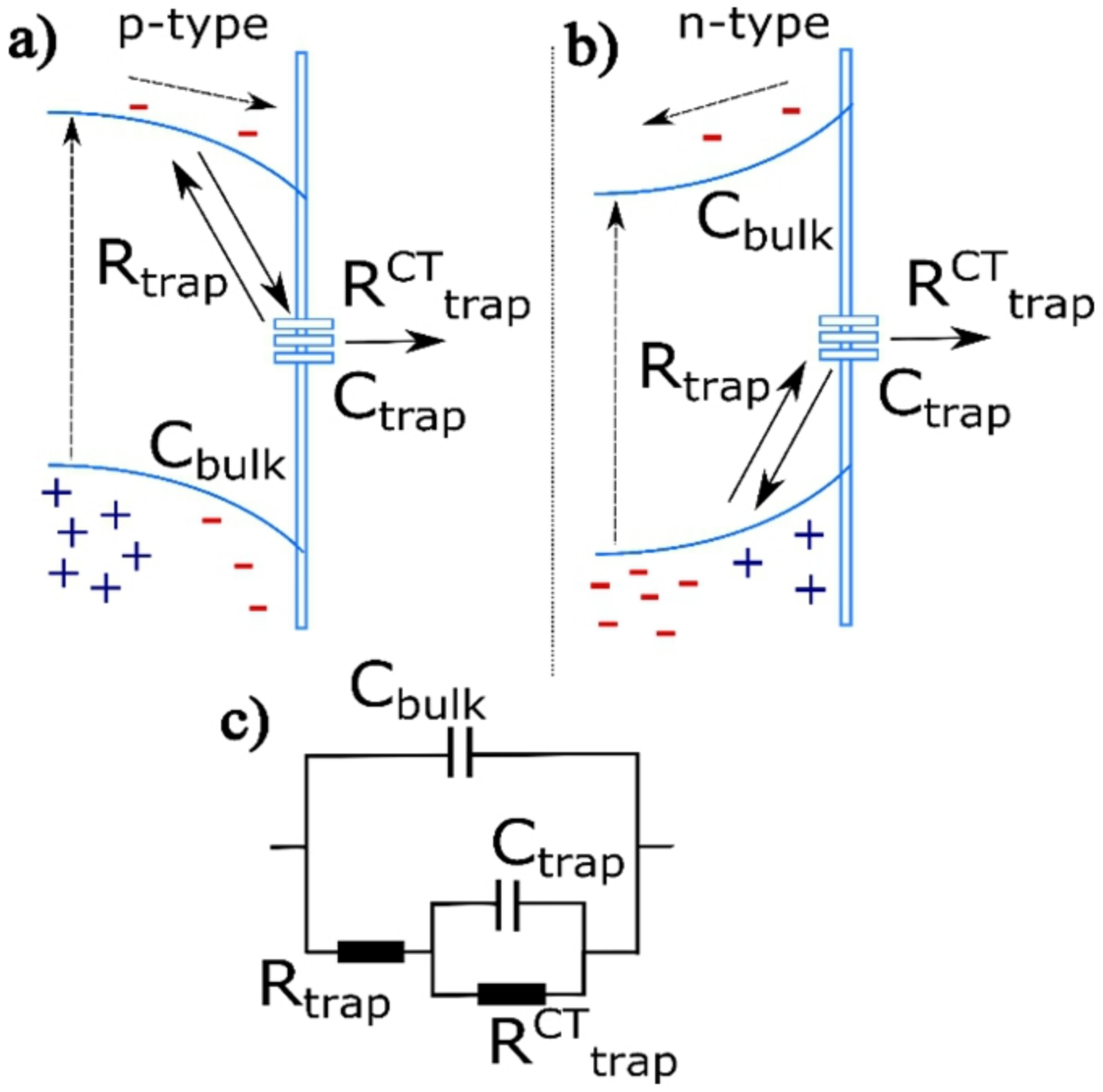
a)
p-type
R_{trap}
R^{CT}_{trap}
C_{trap}
C_{bulk}
b)
n-type
C_{bulk}
R^{CT}_{trap}
R_{trap}
C_{trap}
c)
C_{bulk}
C_{trap}
R_{trap}
R^{CT}_{trap}

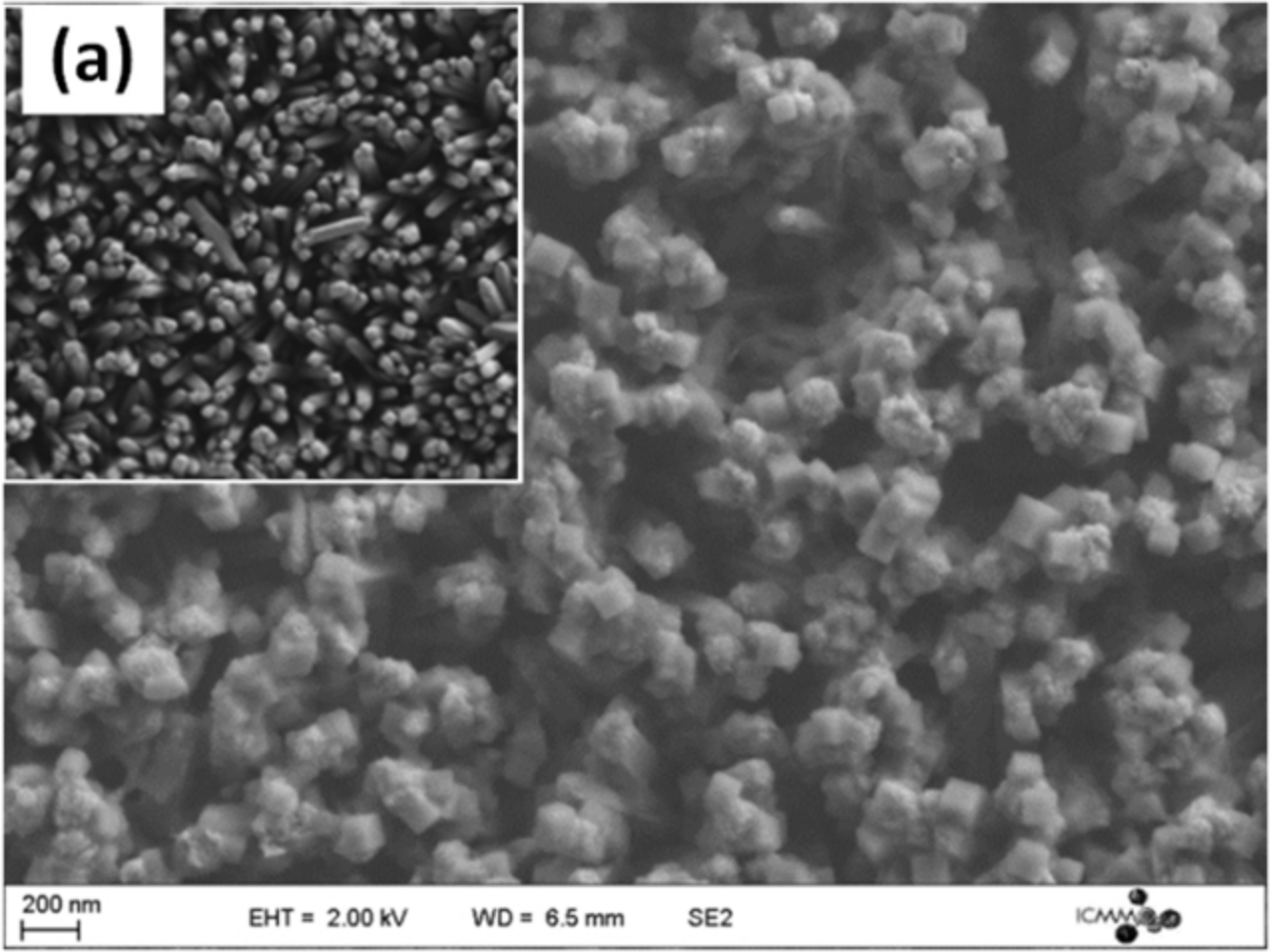
(a)
200 nm
EHT = 2.00 kV
WD = 6.5 mm
SE2

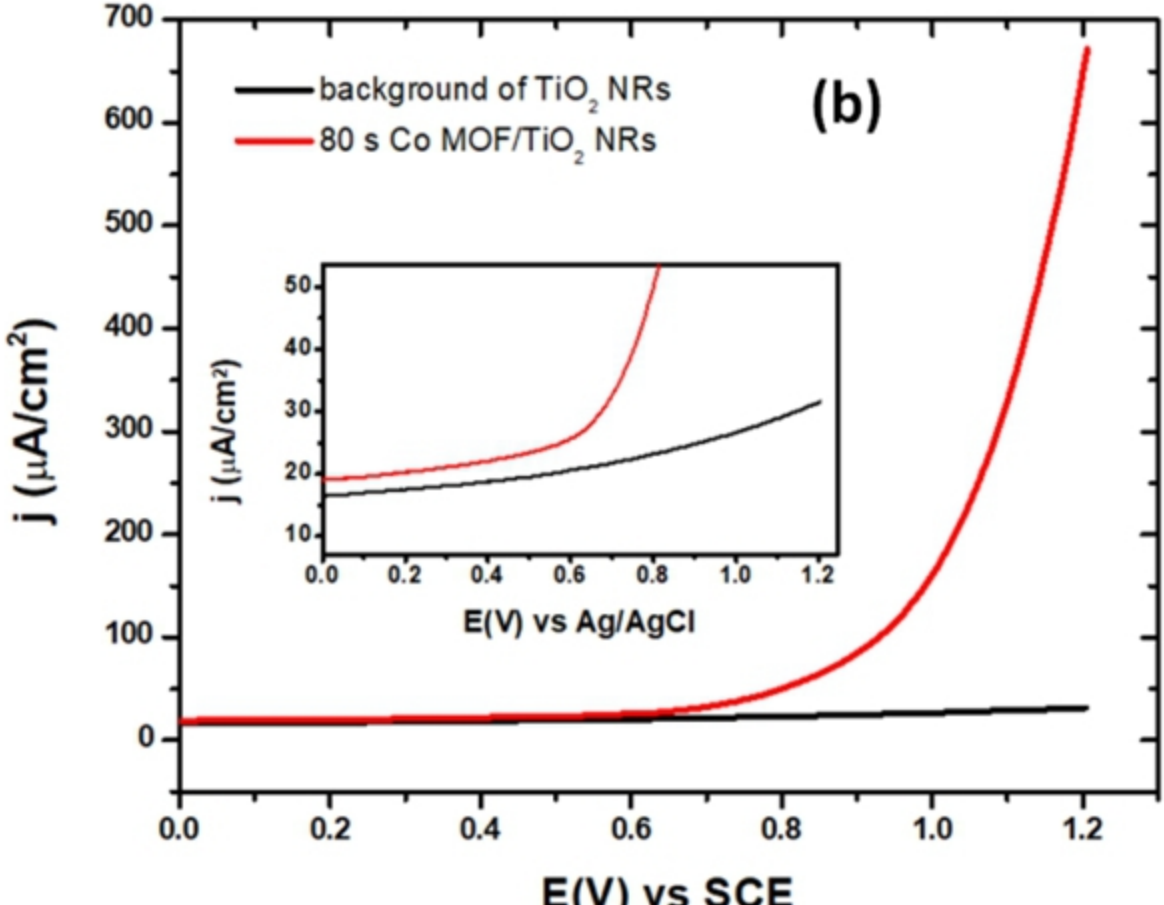
background of TiO2 NRs
80 s Co MOF/TiO2 NRs
(b)
j (μA/cm2)
E(V) vs SCE
700
600
500
400
300
200
100
0
0.0
0.2
0.4
0.6
0.8
1.0
1.2
j (μA/cm2)
E(V) vs Ag/AgCl
50
40
30
20
10
0.0
0.2
0.4
0.6
0.8
1.0
1.2

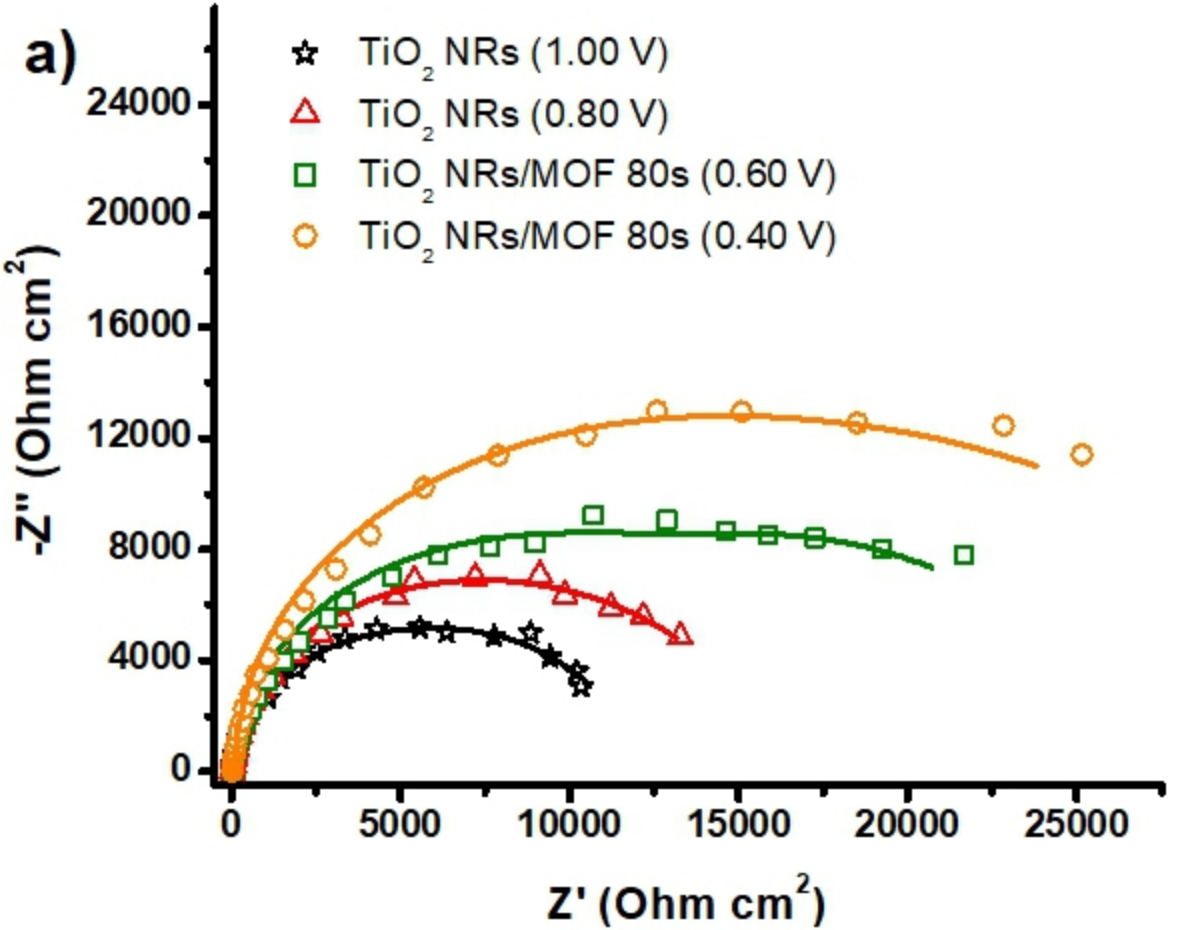
a)
TiO2 NRs (1.00 V)
TiO2 NRs (0.80 V)
TiO2 NRs/MOF 80s (0.60 V)
TiO2 NRs/MOF 80s (0.40 V)
-Z'' (Ohm cm2)
Z' (Ohm cm2)
0
4000
8000
12000
16000
20000
24000
0
5000
10000
15000
20000
25000

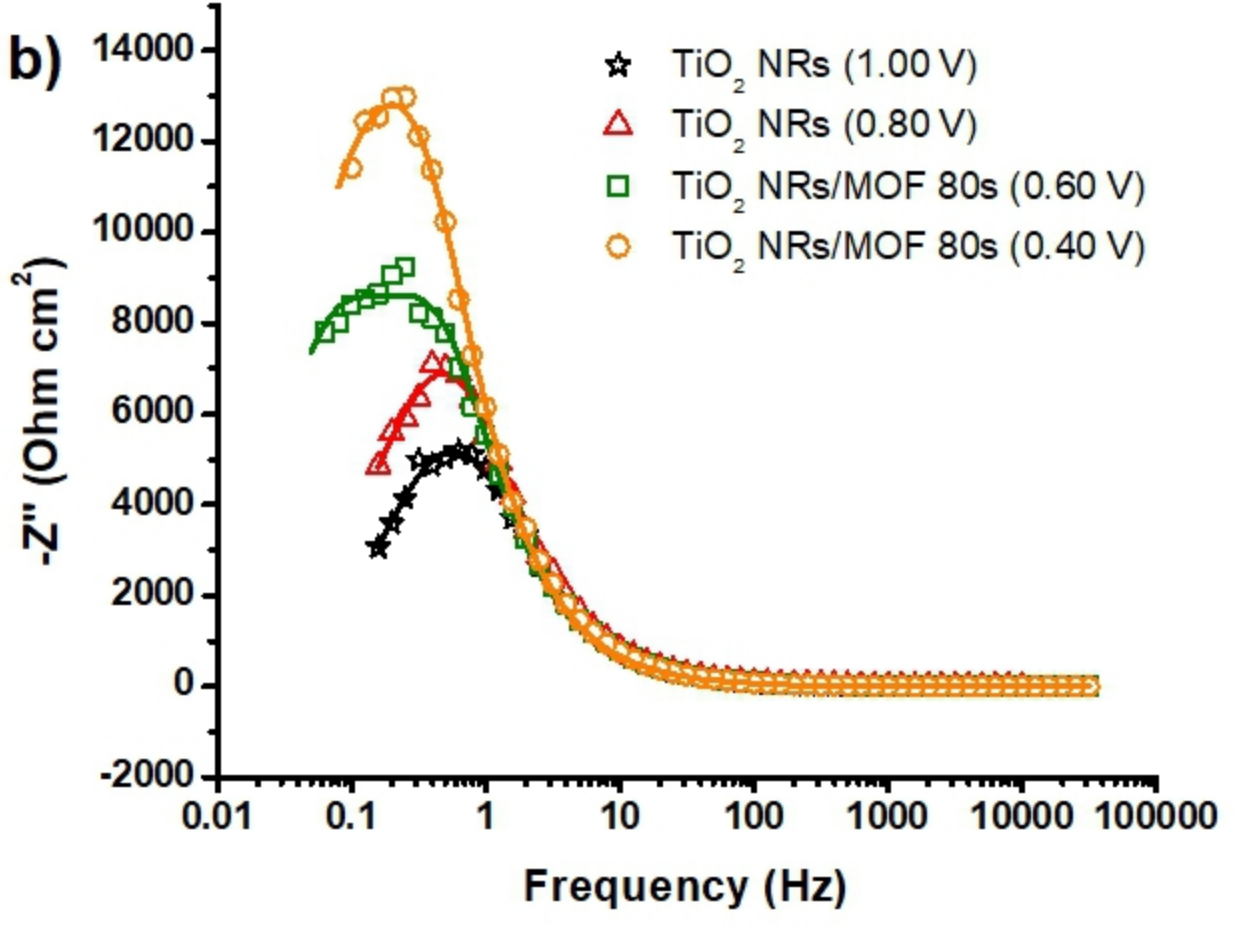
b)
14000
12000
10000
8000
6000
4000
2000
0
-2000
-Z'' (Ohm cm2)
0.01
0.1
1
10
100
1000
10000
100000
Frequency (Hz)
TiO2 NRs (1.00 V)
TiO2 NRs (0.80 V)
TiO2 NRs/MOF 80s (0.60 V)
TiO2 NRs/MOF 80s (0.40 V)

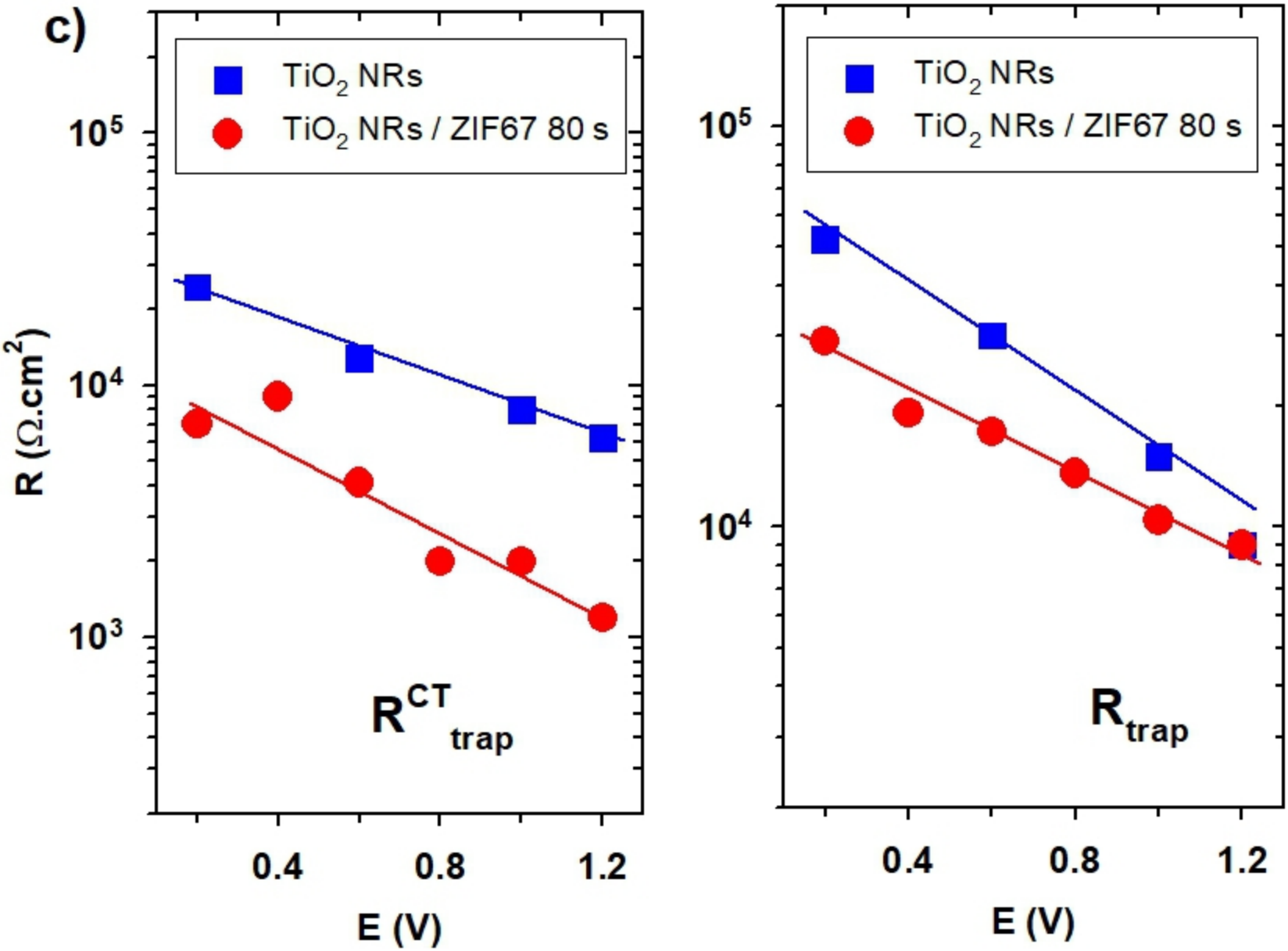
c)
TiO2 NRs
TiO2 NRs / ZIF67 80 s
10^5
10^4
10^3
R (Ω.cm^2)
R^CT trap
0.4
0.8
1.2
E (V)
TiO2 NRs
TiO2 NRs / ZIF67 80 s
10^5
10^4
R trap
0.4
0.8
1.2
E (V)

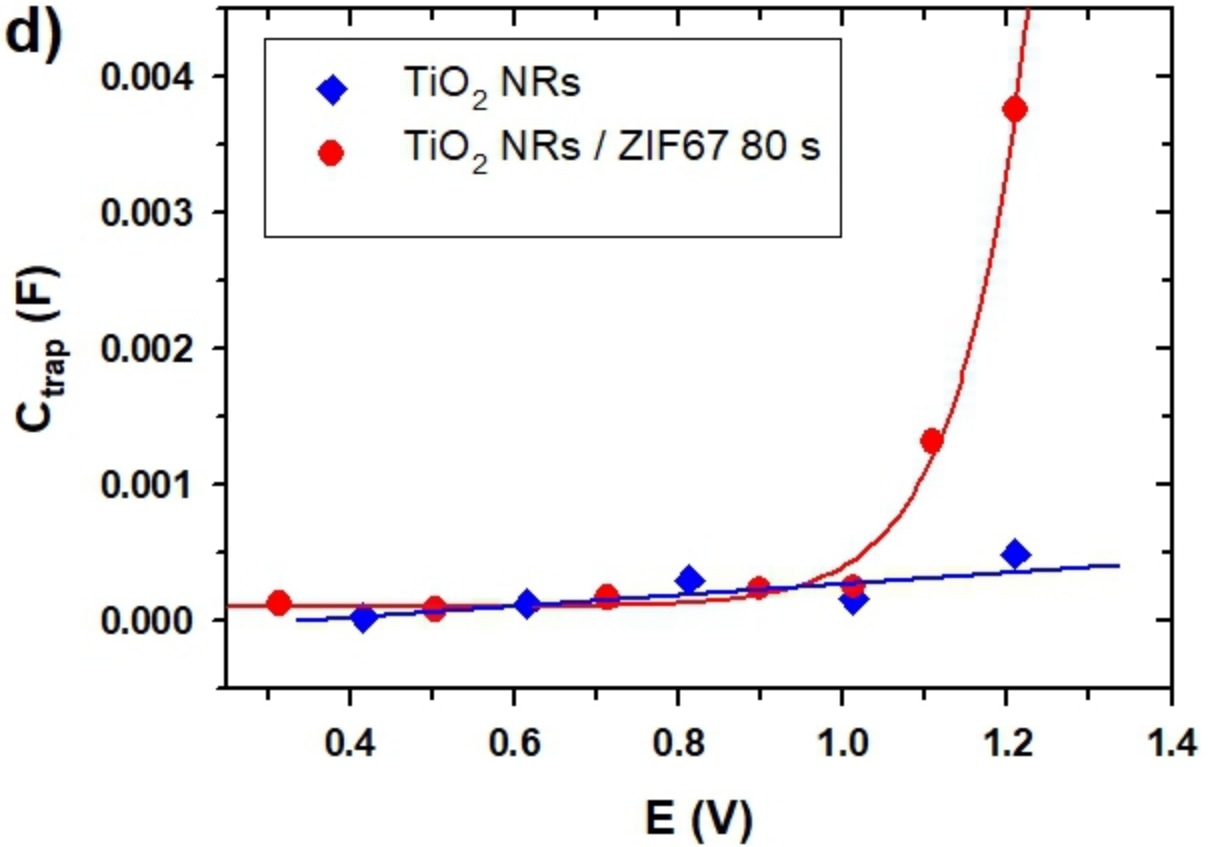
d)
TiO2 NRs
TiO2 NRs / ZIF67 80 s
Ctrap (F)
0.004
0.003
0.002
0.001
0.000
0.4
0.6
0.8
1.0
1.2
1.4
E (V)

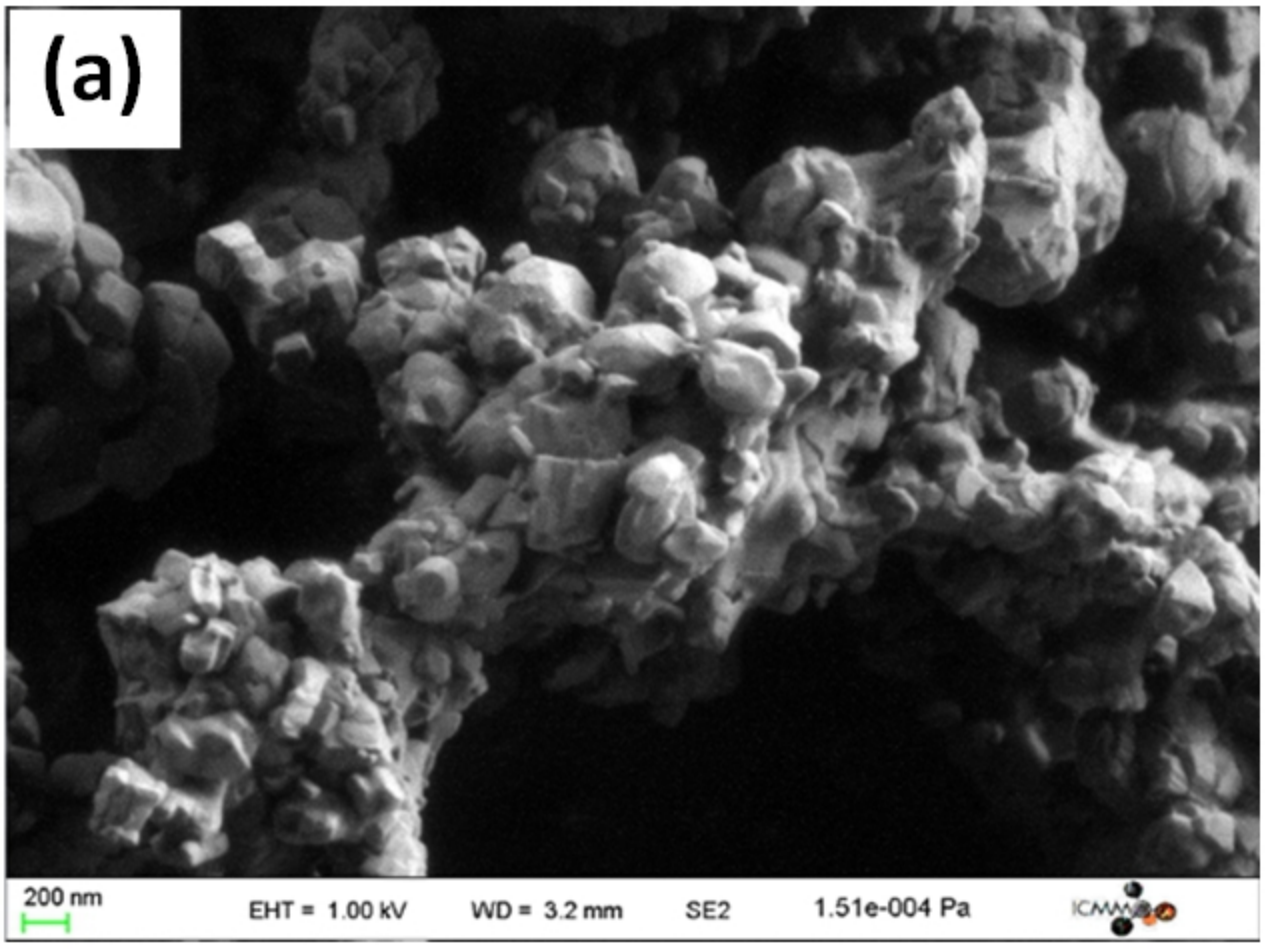
(a)
200 nm
EHT = 1.00 kV
WD = 3.2 mm
SE2
1.51e-004 Pa

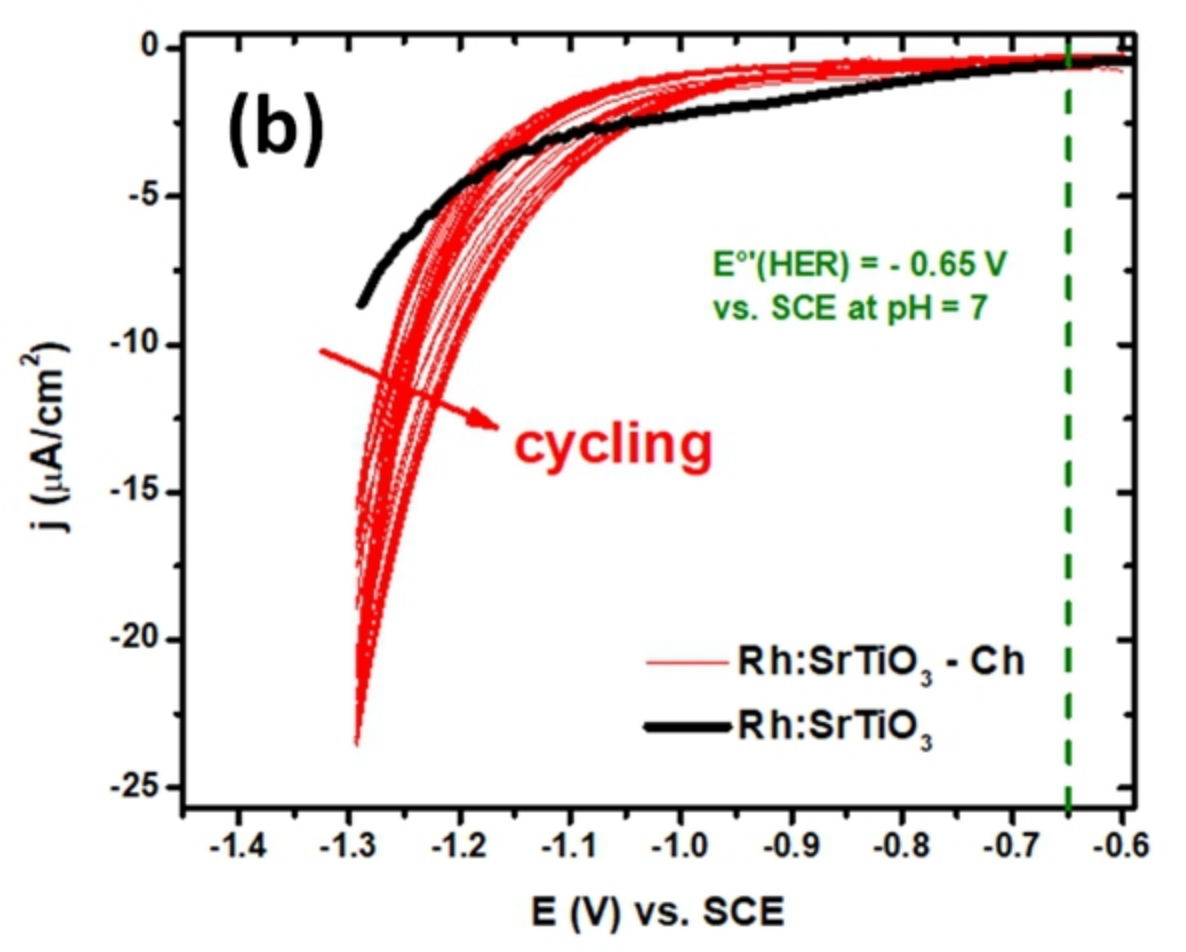
(b)
E°'(HER) = - 0.65 V
vs. SCE at pH = 7
cycling
Rh:SrTiO3 - Ch
Rh:SrTiO3
j (μA/cm2)
E (V) vs. SCE
0
-5
-10
-15
-20
-25
-1.4
-1.3
-1.2
-1.1
-1.0
-0.9
-0.8
-0.7
-0.6

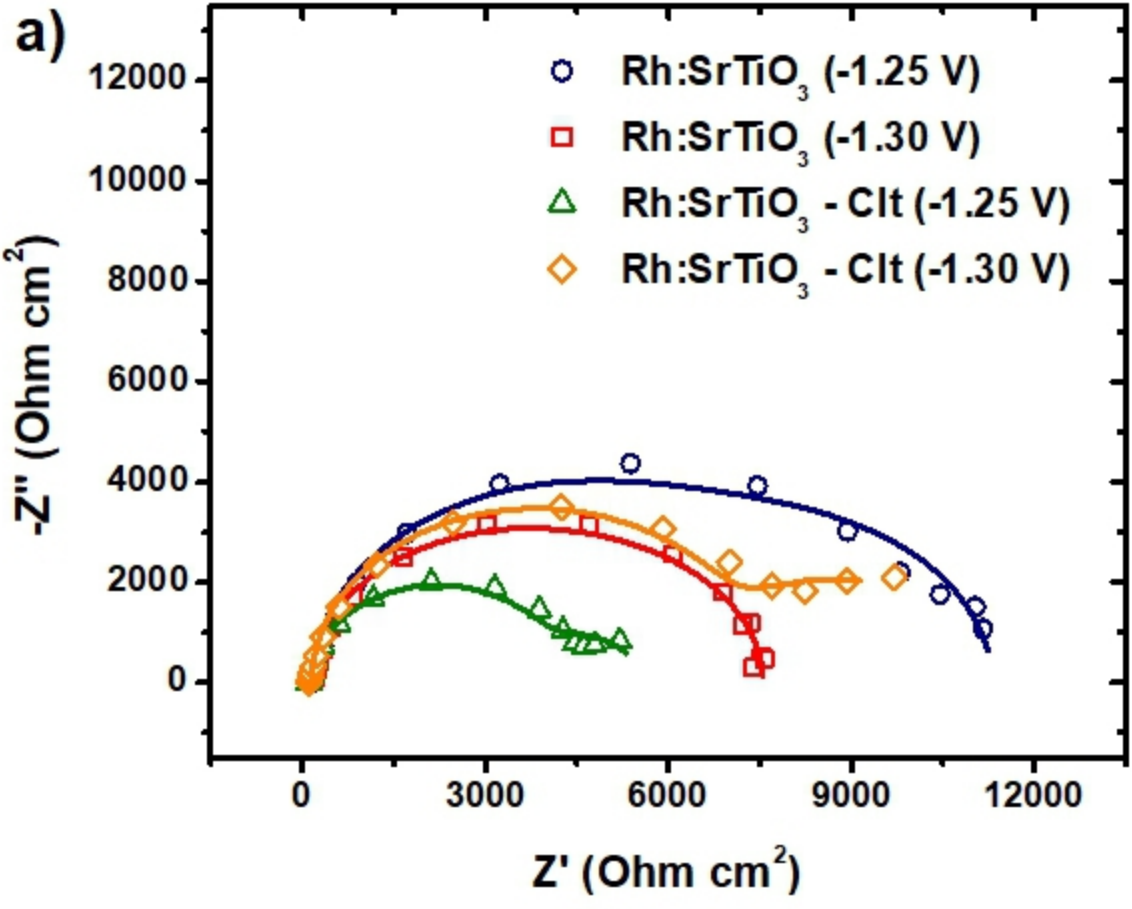
a)
Rh:SrTiO3 (-1.25 V)
Rh:SrTiO3 (-1.30 V)
Rh:SrTiO3 - Clt (-1.25 V)
Rh:SrTiO3 - Clt (-1.30 V)
-Z'' (Ohm cm2)
Z' (Ohm cm2)
0
2000
4000
6000
8000
10000
12000
0
3000
6000
9000
12000

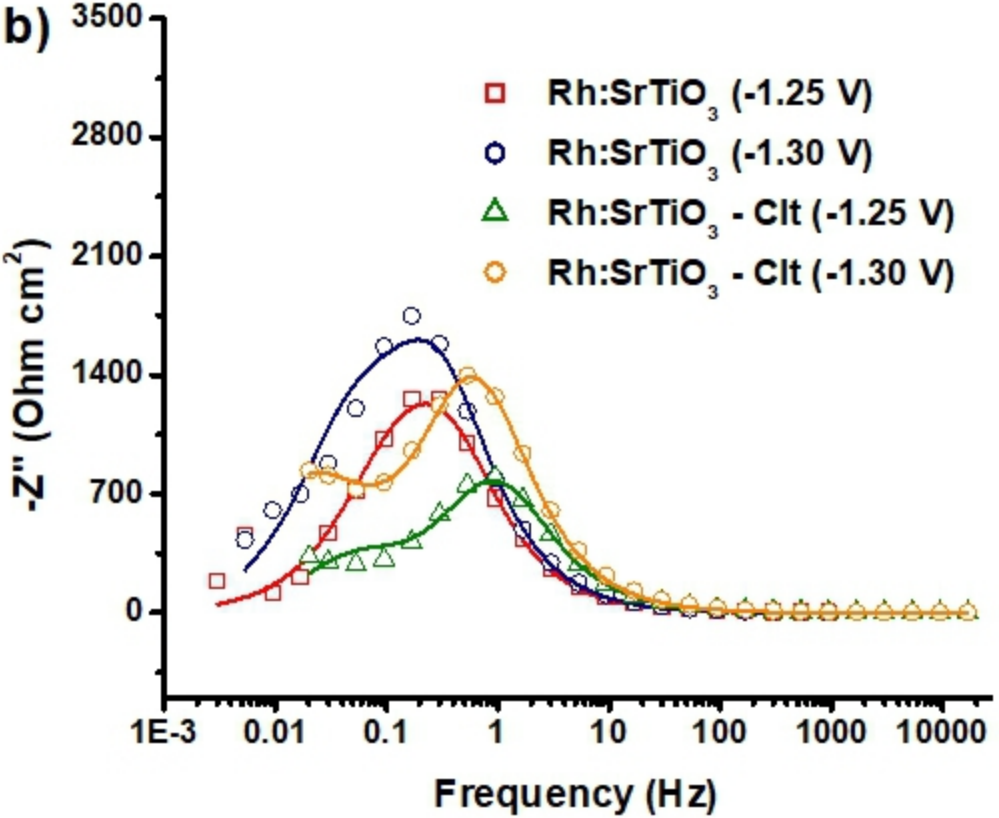
b)
3500
2800
2100
1400
700
0
-Z'' (Ohm cm2)
Rh:SrTiO3 (-1.25 V)
Rh:SrTiO3 (-1.30 V)
Rh:SrTiO3 - Clt (-1.25 V)
Rh:SrTiO3 - Clt (-1.30 V)
1E-3
0.01
0.1
1
10
100
1000
10000
Frequency (Hz)

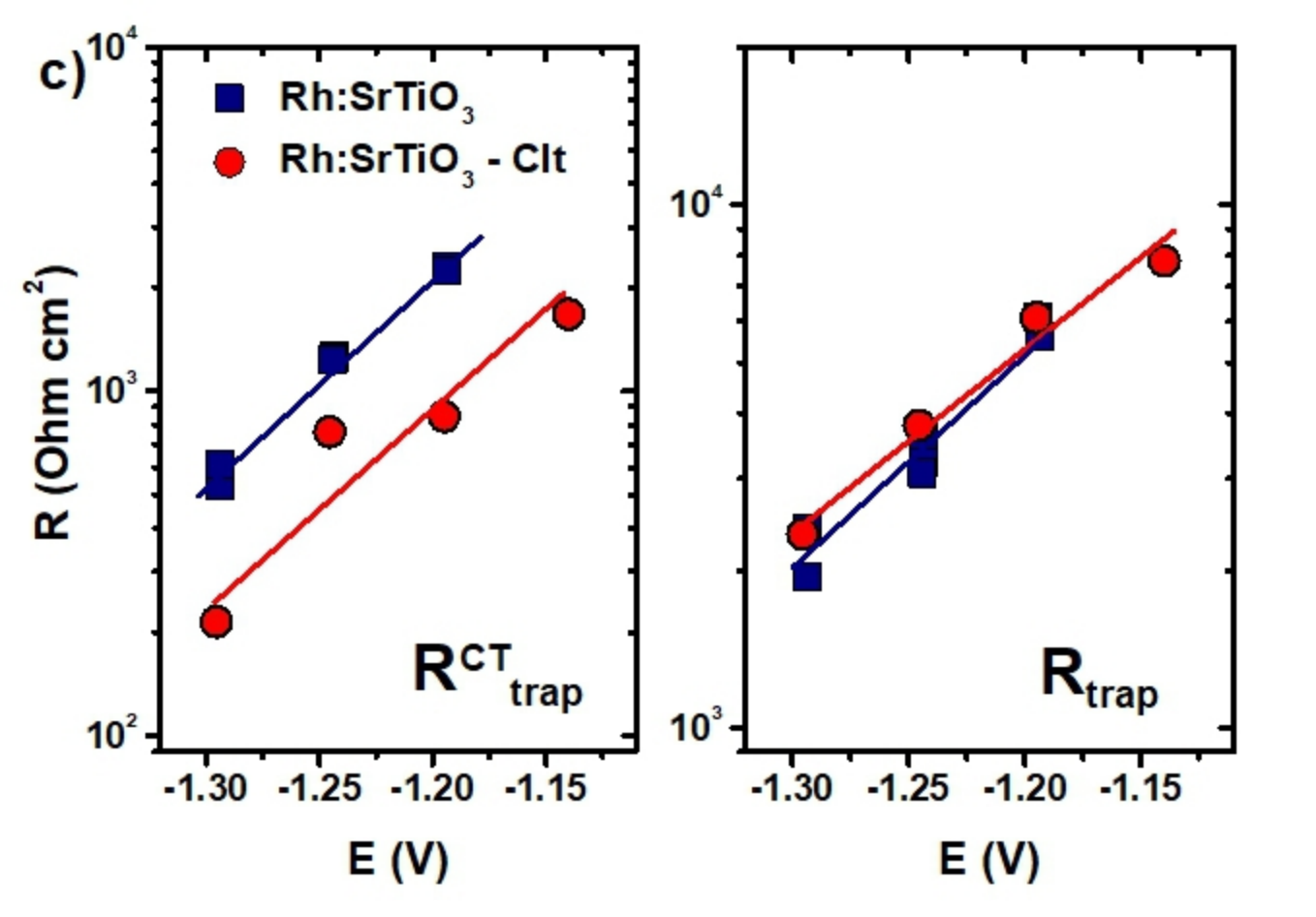
c)
Rh:SrTiO3
Rh:SrTiO3 - Clt
R (Ohm cm2)
10^4
10^3
10^2
R^CT trap
-1.30
-1.25
-1.20
-1.15
E (V)
10^4
10^3
R trap
-1.30
-1.25
-1.20
-1.15
E (V)

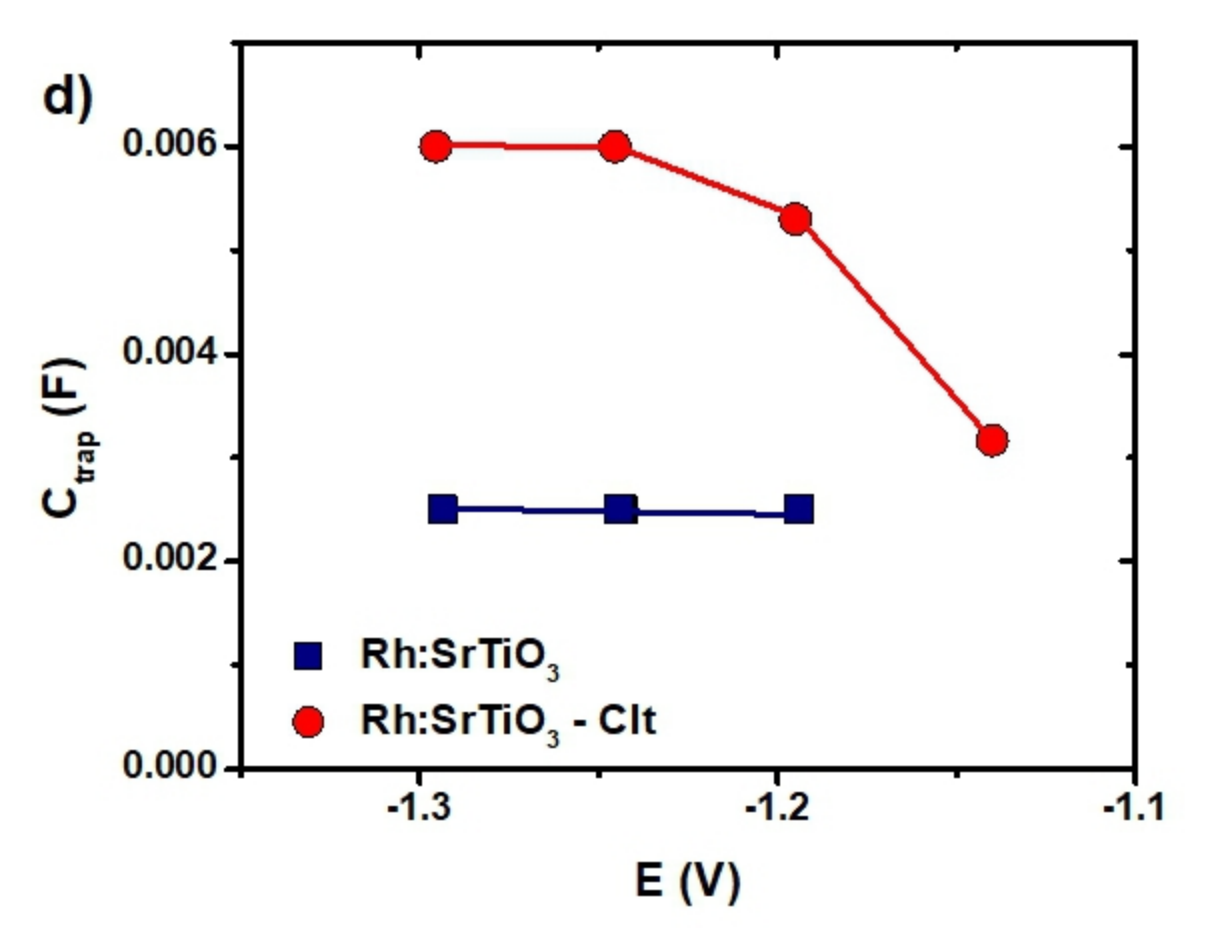
d)
0.006
0.004
0.002
0.000
C_{trap} (F)
Rh:$SrTiO_3$
Rh:$SrTiO_3$ - Clt
-1.3
-1.2
-1.1
E (V)